ACS OMEGA

http://pubs.acs.org/journal/acsodf

Article

Large Magnetodielectric Effect of $BaTiO_3$–$BaFe_{12}O_{19}$ Composites in a Low Magnetic Field

Zijing Dong,* Yongping Pu,* and Guodong Shen

Cite This: *ACS Omega* 2022, 7, 45381–45385

Read Online

ACCESS | Metrics & More | Article Recommendations

ABSTRACT: A microwave sintering procedure has been developed to achieve high quality multiferroic composites of $(1-x)BaTiO_3$–$xBaFe_{12}O_{19}$ (x = 0.05, 0.10, 0.15, and 0.20). X-ray diffraction, scanning electron microscopy, and impedance spectra indicate that $BaFe_{12}O_{19}$ particles are isolated homogeneously by $BaTiO_3$ particles. In a 1.8 T magnetic field, a large room temperature magnetodielectric effect over 4.3% is observed in the $0.8BaTiO_3$–$0.2BaFe_{12}O_{19}$ composite. The total mechanical energy dissipation (Q^{-1}) for the $BaTiO_3$–$BaFe_{12}O_{19}$ composites was composed of the mechanical damping of $BaFe_{12}O_{19}$, the mechanical damping of $BaTiO_3$, and the loss at the interface. The mechanical damping of $BaFe_{12}O_{19}$ plays the dominant role in the variation of Q^{-1}.

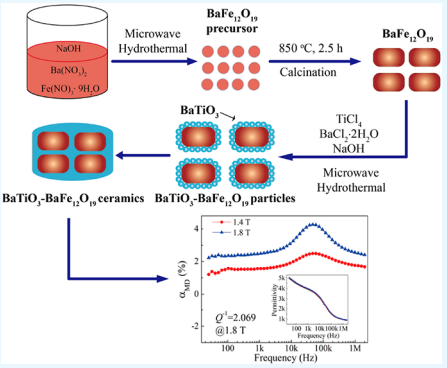

1. INTRODUCTION

With the increasing trends toward device miniaturization, there is escalating interest in multifunctional materials combining both electric and magnetic properties to produce a single device component that can perform more than one task.[1−3] In these multiferroic materials, a sensitive response of dielectric constant to magnetic fields, namely the magnetodielectric (MD) effect, can be used to detect a multiferroic state.[4−6] These product properties based on a multiferroic composite with high MD effect have been projected to find many attractive practical applications like spin-charge transducers, tunable filters, magnetic probes, and novel sensors.[7,8] However, from the fundamental point of view, the MD effect of materials usually occurs at low temperatures or in large magnetic fields.[1,9] Jung et al.[10] have fabricated core/shell $BaTiO_3/\gamma$-Fe_2O_3 nanoparticles, and the percentage change in the dielectric permittivity upon application of 7 T magnetic field was about 1.2% at 200 K. Xu et al.[6] prepared $BaFe_{10.2}Sc_{1.8}O_{19}$ epitaxial thin films, and the maximum value of the magneto-capacitance effect is ∼−2.5% upon application of 8 T magnetic field at 300 K. Thus, one of the most critical issues in this research field is to find the materials with large MD effect in low magnetic fields near room temperature, which makes it possible for practical applications.

A large magnetoelectric effect has been reported in composites of 75 wt % $BaTiO_3$–25 wt % $BaFe_{12}O_{19}$[11] (magnetoelectric coupling coefficients is 2.95 mV/cm at 3 kOe), but few efforts were concentrated on the MD effect. The MD effect of multiferroic composites depends greatly on details of the component phase properties, phase connectivity and uniformity, volume fraction, grain shape, etc. To obtain good composites with a large MD effect in low magnetic fields near room temperature, we take concrete steps in the following direction: (1) choose $BaTiO_3$–$BaFe_{12}O_{19}$ systems to study because of the large piezoelectric and piezomagnetic coefficients of $BaTiO_3$ and $BaFe_{12}O_{19}$ could guarantee a strong magnetoelectric coupling; (2) make $BaTiO_3$ grow around $BaFe_{12}O_{19}$ particle by two-step microwave hydrothermal method, which will maximize the interfacial area between the two phases; (3) use microwave sintering to overcome the nonuniformity of the composites.

To evaluate the MD effect more reasonably, the dissipations in magnetic, electric and mechanical sections should be considered. F. Yang et al. performed the theoretical research on the resonant magnetoelectric effect, and the results indicate that the mechanical dissipation plays a primary role in dissipating resonant status.[12] The mechanical dissipation of material can be characterized by mechanical dissipation factor Q^{-1}, and it is mainly caused by internal friction in the material.[12] In our study, little effort has been devoted to studying the variation of the mechanical energy dissipation Q^{-1} for $BaTiO_3$–$BaFe_{12}O_{19}$ composites, including the mechanical

Received: September 15, 2022
Accepted: November 18, 2022
Published: December 2, 2022

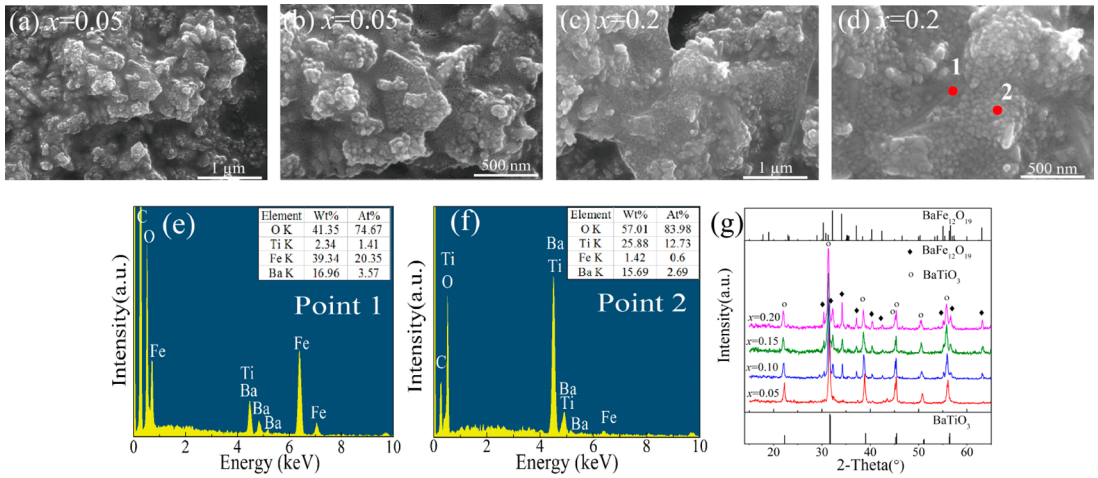

Figure 1. (a, c) SEM micrographs of $(1 - x)BaTiO_3–xBaFe_{12}O_{19}$ powders (x = 0.05, 0.20) with (b, d) enlarged view; (e, f) EDS elemental analysis corresponding to the points in (d); (g) XRD patterns of $(1 - x)BaTiO_3–xBaFe_{12}O_{19}$ ceramics (x = 0.05, 0.10, 0.15, 0.20).

damping of $BaFe_{12}O_{19}$, the mechanical damping of $BaTiO_3$, and the loss at the interface.

This paper aims to develop $BaTiO_3–BaFe_{12}O_{19}$ composites with a significant MD effect in low magnetic fields near room temperature. The MD effect and the mechanical energy dissipation in this system have also been studied and presented.

2. MATERIALS AND METHODS

$(1 - x)BaTiO_3–xBaFe_{12}O_{19}$ (x = 0.05, 0.10, 0.15 and 0.20, x represents mole fraction) particles were synthesized by a two-step microwave hydrothermal method. Our modified two-step method was to first synthesize the $BaFe_{12}O_{19}$ powder by a microwave hydrothermal method and then mix it with $BaTiO_3$ precursor. The solution in a sealed tetrafluorometoxil vessel was heated at 180 °C for 30 min. Details of the processing conditions can be found in our previous work.[13] $BaTiO_3–BaFe_{12}O_{19}$ ceramics were prepared by microwave sintering at 1100 °C in air for 45 s. All the ceramics have shown a high relative density (>95%).

The phase composition of the samples was determined by X-ray powder diffraction (XRD, Rigaku, Tokyo, Japan). The morphology of the samples was observed using the scanning electron microscopy (SEM, Hitachi S4800). Magnetic hysteresis loops were measured at room temperature on a Quantum Design PPMS-9T with a vibrating sample magnetometer. The polarization hysteresis loops were characterized by a ferroelectric test system (Premier II, Radiant, USA). The permittivity and magnetodielectric effect of the present ceramics were evaluated in a frequency range 20 Hz-2 MHz using a precision LCR Meter (Model: E4980A, Agilent Tech., CA). An electromagnet provided the dc magnetic fields H from 1.4 to 1.8 T.

3. RESULTS AND DISCUSSION

The SEM micrographs of $(1 - x)BaTiO_3–xBaFe_{12}O_{19}$ (x = 0.05 and 0.20) nanoparticles are presented in Figure 1a–d. In previous studies, $BaFe_{12}O_{19}$ particles prepared by the microwave hydrothermal method possess flat planes in shape and $BaTiO_3$ particles display a spherical shape.[14] In Figure 1a–d, there are many spherical particles around the lamellae, which means several $BaTiO_3$ crystallites may epitaxially grow on one $BaFe_{12}O_{19}$ nanoparticle in the second step of the microwave hydrothermal reaction. The existence of this microstructure in these samples is well supported by the EDS analysis (Figure 1e,f): Fe, Ba, and O elements are detected in point 1(lamellae $BaFe_{12}O_{19}$), whereas Ba, Ti, and O dominate point 2 (spherical $BaTiO_3$). Figure 1g shows the XRD patterns of $BaTiO_3–BaFe_{12}O_{19}$ ceramics. Only $BaTiO_3$ and $BaFe_{12}O_{19}$ crystal phases are observed, indicating that no intermediate phase formed at the interface between $BaTiO_3$ and $BaFe_{12}O_{19}$ either during the microwave hydrothermal synthesis or after microwave sintering.

Fractured surface of $BaTiO_3–BaFe_{12}O_{19}$ ceramics are examined with SEM, as shown in Figure 2. All ceramics show much higher density and homogeneous microstructure. The average grain size of the composites increases with the increase of ferrite content in the composites.

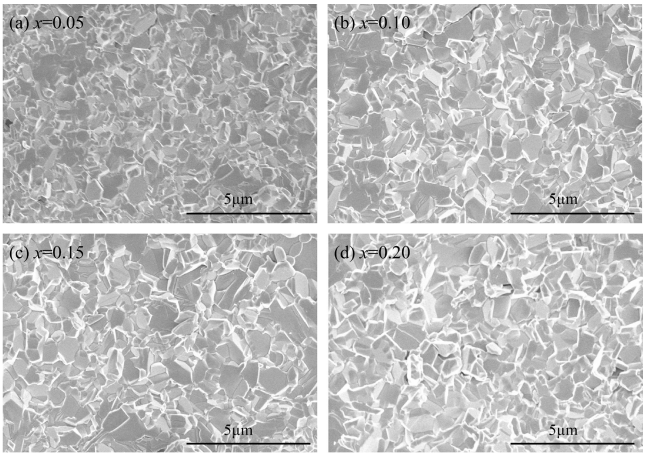

Figure 2. SEM micrographs of fracture surface of $BaTiO_3–BaFe_{12}O_{19}$ ceramics with $BaFe_{12}O_{19}$ of (a) 0.05, (b) 0.10, (c) 0.15, and (d) 0.20.

For many dielectrics, especially ferroelectric ceramics, helpful information can be obtained from maxima in spectra of the imaginary component of the electric modulus (M''). The maxima in M'' spectra are dominated by components with the smallest capacity value.[15] M'' as a function of frequency at different temperatures are plotted in Figure 3. Two M'' peaks could be clearly observed with the one at the low-frequency region (peak I) and the other at high frequency region (peak

https://doi.org/10.1021/acsomega.2c05975
ACS Omega 2022, 7, 45381−45385

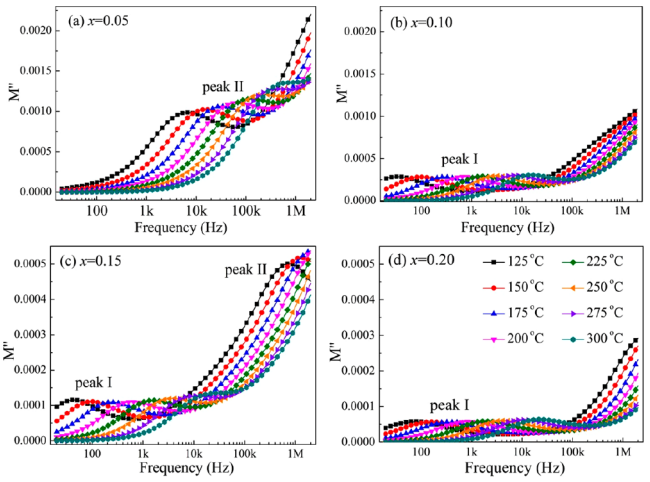

Figure 3. Frequency dependence of M'' for $(1-x)BaTiO_3-xBaFe_{12}O_{19}$ ceramics at various temperatures: (a) x = 0.05, (b) x = 0.10, (c) x = 0.15, and (d) x = 0.20.

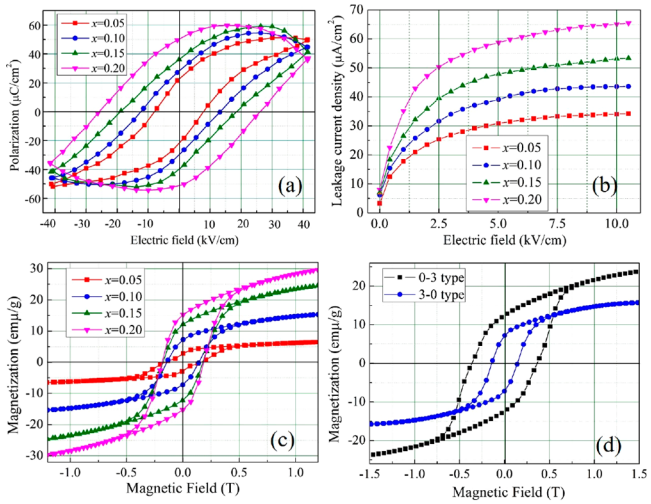

Figure 4. (a) Polarization hysteresis loops for $BaTiO_3-BaFe_{12}O_{19}$ ceramics, (b) leakage current density versus applied electric field for $BaTiO_3-BaFe_{12}O_{19}$ ceramics, (c) magnetic hysteresis loops for $BaTiO_3-BaFe_{12}O_{19}$ ceramics at room temperature, and (d) magnetic hysteresis loops of 3−0 type and 0−3 type $0.90BaTiO_3-0.10BaFe_{12}O_{19}$ composites.

II). The peak I response can be attributed to a long-range conduction process, and the peak II response is associated with a short-range relaxation process.[16] The position of peak I shifts toward high frequencies with increasing temperature indicating a thermally activated conduction process in which the hopping mechanism of charge carriers dominates intrinsically. Interestingly, the value of the peak I response is much lower than that of the peak II response, indicating that the long-range migration of charge carriers is weaker than the short-range migration of charge carriers. As shown in Figure 1, $BaFe_{12}O_{19}$ particles are surrounded by plenty of $BaTiO_3$ crystallites. Since $BaTiO_3$ is far more electrically insulating than $BaFe_{12}O_{19}$, the microstructure mentioned above will hinder the long-range migration of charge carriers, leading to the low value of the peak I response.

The polarization hysteresis ($P-E$) loops of the $BaTiO_3-BaFe_{12}O_{19}$ ceramics with different contents of $BaFe_{12}O_{19}$ are shown in Figure 4(a). Observation of $P-E$ loops confirms the ferroelectric nature of all the composites at room temperature. The measured $P-E$ data contain the contributions from leakage current, free charge carriers, switched charge density, etc. The $P-E$ loops become more and more round with increasing $BaFe_{12}O_{19}$ content due to the presence of large leakage current. For more detailed description, the $I-E$ curves of the $BaTiO_3-BaFe_{12}O_{19}$ composites at room temperature are shown in Figure 4b. The leakage current density increases with increasing $BaFe_{12}O_{19}$ content, which is consistent with the above $P-E$ loops analysis results. $BaFe_{12}O_{19}$ has a large leakage current density relative to $BaTiO_3$, due to its lower resistivity. Therefor, The increase of the leakage current density can be attributed to the presence of $BaFe_{12}O_{19}$.

Figure 4c shows the room temperature magnetic hysteresis loops of $BaTiO_3-BaFe_{12}O_{19}$ ceramics. All samples show good ferromagnetic behavior because of the ordered magnetic structure in the composites. The saturation magnetization, remanent magnetization, and coercivity of samples increase with increasing $BaFe_{12}O_{19}$ content. This increase of the magnetization can be attributed to the presence of magnetic phase $BaFe_{12}O_{19}$. $BaTiO_3$ is a nonmagnetic material, and the magnetic phase $BaFe_{12}O_{19}$ is the main body to supply magnetism, so the increase of $BaFe_{12}O_{19}$ content leads to the increase of magnetization. To studied the ferromagnetic properties of $BaTiO_3-BaFe_{12}O_{19}$ composites with different microstructure, magnetic hysteresis loops for 3−0 type $0.90BaTiO_3-0.10BaFe_{12}O_{19}$ composite ceramics ($BaTiO_3$ crystallites epitaxially grow on the $BaFe_{12}O_{19}$ nanoparticle) and 0−3 type $0.90BaTiO_3-0.10BaFe_{12}O_{19}$ composite ceramics ($BaFe_{12}O_{19}$ grows on the $BaTiO_3$ nanoparticle) are shown in Figure 4d. As compared with the magnetic properties of the two samples, the 0−3 type sample exhibits higher magnetization value and higher coercivity at room temperature, because of $BaFe_{12}O_{19}$ in 0−3 type composites has much stronger interactions between each other.

In order to investigate the MD effect in the system, the frequency dependencies of the MD effect at different magnetic fields (1.4 and 1.8 T) are presented in Figure 5, and the frequency dependence of dielectric permittivity for the samples

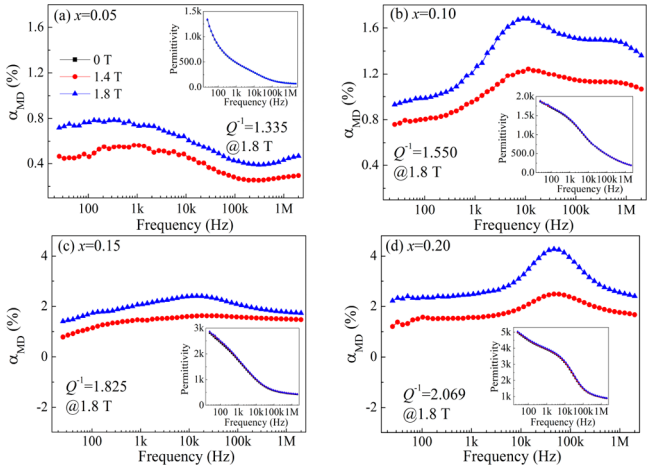

Figure 5. Frequency dependence of magnetodielectric coefficient (α_{MD}) for $(1-x)BaTiO_3-xBaFe_{12}O_{19}$ ceramics at different magnetic fields: (a) x = 0.05, (b) x = 0.10, (c) x = 0.15, and (d) x = 0.20. The inset shows the frequency dependence of permittivity for the samples at different magnetic fields.

https://doi.org/10.1021/acsomega.2c05975
ACS Omega 2022, 7, 45381−45385

at different magnetic fields are shown in the inset of Figure 5. The MD effect is defined as

$$\alpha_{MD} = [\varepsilon(H) - \varepsilon(0)]/\varepsilon(0) \times 100\% \quad (1)$$

where α_{MD} is the magnetodielectric coefficient, $\varepsilon(H)$ and $\varepsilon(0)$ are permittivity at magnetic field H and 0 at the same frequency. The MD response is found to increase with the increasing content of the magnetic phase. A maximum of α_{MD} reaches up to ~4.3% for the composite with $x = 0.20$ at room temperature and 46.6 kHz electric field frequency in the presence of a 1.8 T magnetic field. The observed MD behavior under an external magnetic field is contributed due to the magnetostriction in the magnetic phase produces stresses that are transferred to the ferroelectric phase, resulting in an electric polarization of this phase.[17,18] This behavior can be significantly enhanced near the electromechanical resonance frequency f_r (EMR frequency).[8]

Clearly, the value of α_{MD} at a resonance frequency f_r comes up to a maximum as indicated by Figure 5. Magnetomechanical resonance is a resonant phenomenon caused by magnetostriction vibration during magnetization. When the frequency is near f_r, the strength of magnetomechanical resonance achieves a maximum, which means the magnetostriction effect reached the maximum. As we mentioned above, MD behavior strongly depends on the magnetostriction effect of $BaTiO_3$–$BaFe_{12}O_{19}$ composites, the value of α_{MD} at f_r comes up to a maximum.

The fact that all α_{MD} values are lower than predicted can be attributed to a variety of factors, including the formation of cracks[19] or mechanical energy dissipation[20] at the interface between the two phases. The total mechanical energy dissipation (Q^{-1}) is defined as[8]

$$Q^{-1} = \Delta f_r / f_r \quad (2)$$

where Δf_r is the 3 dB frequency bandwidth and f_r is the EMR frequency. The relevant data are referenced in Table 1. In the

Table 1. Q^{-1}, Δf_r, and f_r of $(1-x)BaTiO_3$–$xBaFe_{12}O_{19}$ (x = 0.05, 0.10, 0.15, 0.20) Composites Measured at a 1.8 T Magnetic Field

$BaFe_{12}O_{19}$ content	Q^{-1}	Δf_r (Hz)	f_r (Hz)
0.05	1.335	1146.307	858.4
0.10	1.550	13848.049	8997
0.15	1.825	26257.433	14390
0.20	2.069	96429.380	46600

presence of a 1.8 T magnetic field, Q^{-1} increases from 1.335 to 2.069 with the addition of $BaFe_{12}O_{19}$ from 0.05 to 0.20 for the $BaTiO_3$–$BaFe_{12}O_{19}$ composite. In this paper, we define Q^{-1} as mainly composed of the mechanical damping of $BaFe_{12}O_{19}$ ($Q_{mech,BFO}^{-1}$), mechanical damping of $BaTiO_3$ ($Q_{mech,BT}^{-1}$), and the loss at the interface ($Q_{interface}^{-1}$). In this way, Q^{-1} can be expressed as

$$\begin{aligned} Q^{-1} &= \Delta f_r / f_r \\ &= xQ_{mech,BFO}^{-1} + (1-x)Q_{mech,BT}^{-1} + Q_{interface}^{-1} \\ &= x(Q_{mech,BFO}^{-1} + Q_{interface}^{-1}) + (1-x)(Q_{mech,BT}^{-1} + Q_{interface}^{-1}) \end{aligned} \quad (3)$$

In view of eq 3 being a linear equation with two different variables such as $Q_{mech,BFO}^{-1} + Q_{interface}^{-1}$ and $Q_{mech,BT}^{-1} + Q_{interface}^{-1}$, we can calculate $Q_{mech,BFO}^{-1} + Q_{interface}^{-1}$ and $Q_{mech,BT}^{-1} + Q_{interface}^{-1}$ for different $BaFe_{12}O_{19}$ content, as shown in Table 2. The

Table 2. Values of $Q_{mech,BFO}^{-1} + Q_{interface}^{-1}$ and $Q_{mech,BT}^{-1} + Q_{interface}^{-1}$ for different $BaFe_{12}O_{19}$ Content (x)

$BaFe_{12}O_{19}$ content	$Q_{mech,BFO}^{-1} + Q_{interface}^{-1}$	$Q_{mech,BT}^{-1} + Q_{interface}^{-1}$
x = 0.05 and x = 0.10	5.426	1.120
x = 0.10 and x = 0.15	6.490	1.002
x = 0.15 and x = 0.20	5.983	1.091

similarity of the three group data proves the self-consistency of our discussion based on eq 3. The calculated value of $Q_{mech,BFO}^{-1} + Q_{interface}^{-1}$ is much higher than $Q_{mech,BT}^{-1} + Q_{interface}^{-1}$, indicating that $Q_{mech,BFO}^{-1}$ plays a dominant role in the variation of mechanical energy dissipation Q^{-1}. This explained why Q^{-1} increases with increasing $BaFe_{12}O_{19}$ content.

4. CONCLUSIONS

In summary, $(1-x)BaTiO_3$–$xBaFe_{12}O_{19}$ (x = 0.05, 0.10, 0.15 and 0.20) composites can be successfully prepared by microwave sintering for 45 s without any intermediate or impurity phase. There is a large MD effect up to 4.3% around the electromechanical resonance frequency in a magnetic field of 1.8 T at room temperature, which mainly originated from the mechanical stress transfer in a magnetic field. The contribution of each loss is clarified via the analysis of the MD effect with different x. It turns out that the mechanical energy dissipation of $BaFe_{12}O_{19}$ plays a dominant role in the variation of mechanical energy dissipation, resulting in the fact that Q^{-1} increases with increasing x.

AUTHOR INFORMATION

Corresponding Authors

Zijing Dong − *School of Textile Science and Engineering, Xi'an Polytechnic University, Xi'an, Shaanxi 710048, China; Key Laboratory of Functional Textile Material and Product (Xi'an Polytechnic University), Ministry of Education, Xi'an, Shaanxi 710048, China;* orcid.org/0000-0001-5255-4441; Email: dongzijing@xpu.edu.cn

Yongping Pu − *School of Materials Science and Engineering, Shaanxi University of Science & Technology, Xi'an 710021, China*; Email: puyongping@sust.edu.cn

Author

Guodong Shen − *School of Textile Science and Engineering, Xi'an Polytechnic University, Xi'an, Shaanxi 710048, China; Key Laboratory of Functional Textile Material and Product (Xi'an Polytechnic University), Ministry of Education, Xi'an, Shaanxi 710048, China*

Complete contact information is available at: https://pubs.acs.org/10.1021/acsomega.2c05975

Notes

The authors declare no competing financial interest.

https://doi.org/10.1021/acsomega.2c05975
ACS Omega 2022, 7, 45381−45385

■ ACKNOWLEDGMENTS

This research was supported by the Natural Science Basic Research Program of Shaanxi (Program No. 2021JQ-691), the Scientific Research Program Funded by Shaanxi Provincial Education Department (Program No. 20JK0652), the Shaanxi Province Innovative Talent Promotion Plan-Science and Technology Innovation Team (No. 2022TD-29), and the Shaanxi Province Key R&D Program Key Industrial Innovation Chain (Cluster)-Social Development Field (No. 2022ZDLSF01-11).

■ REFERENCES

(1) Singh, S.; Kumar, N.; Bhargava, R.; Sahni, M.; Sung, K. J.; Jung, J. H. Magnetodielectric effect in $BaTiO_3/ZnFe_2O_4$ core/shell nanoparticles. *J. Alloy. Compd.* **2014**, *587*, 437−441.

(2) Pradhan, D. K.; Kumari, S.; Rack, P. D. Magnetoelectric composites: applications, coupling mechanisms, and future directions. *Nanomaterials.* **2020**, *10*, 2072.

(3) Omelyanchik, A.; Antipova, V.; Gritsenko, C.; Kolesnikova, V.; Murzin, D.; Han, Y. L.; Turutin, A. V.; Kubasov, I. V.; Kislyuk, A. M.; Ilina, T. S.; Kiselev, D. A.; Voronova, M. I.; Malinkovich, M. D.; Parkhomenko, Y. N.; Silibin, M.; Kozlova, E. N.; Peddis, D.; Levada, K.; Makarova, L.; Amirov, A.; Rodionova, V. Boosting magnetoelectric effect in polymer-based nanocomposites. *Nanomaterials.* **2021**, *11*, 1154.

(4) Vadla, S. S.; Kulkarni, A. R.; Narayanan, V. Magnetoelectric coupling in $0.5Pb(Ni_{1/3}Nb_{2/3})O_3$-$0.35PbTiO_3$-$0.15PbZrO_3$ and $CoFe_2O_4$ based particulate composites. *Scripta Mater.* **2016**, *112*, 140−143.

(5) Rather, G. H.; Rather, M. D.; Nazir, N.; Ikram, A.; Ikram, M.; Want, B. Particulate multiferroic $Ba_{0.99}Tb_{0.02}Ti_{0.99}O_3$-$CoFe_{1.8}Mn_{0.2}O_4$ composites: improved dielectric, ferroelectric and magneto-dielectric properties. *J. Alloy. Compd.* **2021**, *887*, No. 161446.

(6) Xu, S. C.; Zhu, Q. S.; Liang, G. Q.; Zhang, J. M.; Wang, H.; Wang, H. Y.; Zhao, R.; You, L.; Su, X. D.; Tang, R. J. Lattice defects related magnetic and magnetocapacitance properties of multiferroic $BaFe_{10.2}Sc_{1.8}O_{19}$ epitaxial thin films. *Scripta Mater.* **2022**, *210*, No. 114466.

(7) Nan, C. W.; Bichurin, M. I.; Dong, S. X.; Viehland, D.; Srinivasan, G. Multiferroic magnetoelectric composites: Historical perspective, status, and future directions. *J. Appl. Phys.* **2008**, *103*, No. 031101.

(8) Yao, Y. P.; Hou, Y.; Dong, S. N.; Li, X. G. Giant magnetodielectric effect in Terfenol-D/PZT magnetoelectric laminate composite. *J. Appl. Phys.* **2011**, *110*, No. 014508.

(9) Rathore, S. S.; Vitta, S. Large low field room temperature magneto-dielectric response from $(Sr_{0.5}Ba_{0.5})Nb_2O_6/Co(Cr_{0.4}Fe_{1.6})$-$O_4$ bulk 3−0 composites. *Mater. Sci. Eng., B* **2016**, *204*, 1−7.

(10) Koo, Y. S.; Bonaedy, T.; Sung, K. D.; Jung, J. H.; Yoon, J. B.; Jo, Y. H.; Jung, M. H.; Lee, H. J.; Koo, T. Y.; Jeong, Y. H. Magnetodielectric coupling in core/shell $BaTiO_3/\gamma$-Fe_2O_3 nanoparticles. *Appl. Phys. Lett.* **2007**, *91*, 212903.

(11) Srinivas, A.; Raja, M.; Sivaprahasam, D.; Saravanan, P. Enhanced ferroelectricity and magnetoelectricity in $0.75BaTiO_3$-$0.25BaFe_{12}O_{19}$ by spark plasma sintering. *Process. Appl. Ceram.* **2013**, *7*, 29−35.

(12) Yang, F.; Wen, Y. M.; Li, P.; Zheng, M.; Bian, L. X. Resonant magnetoelectric response of magnetostrictive/piezoelectric laminate composite in consideration of losses. *Sensor. Actuat. A-Phys.* **2008**, *141*, 129−135.

(13) Dong, Z. J.; Pu, Y. P.; Gao, Z. Y.; Wang, P. K.; Liu, X. Y.; Sun, Z. X. Fabrication, structure and properties of $BaTiO_3$-$BaFe1_2O_{19}$ composites with core-shell heterostructure. *J. Eur. Ceram. Soc.* **2015**, *35*, 3513−3520.

(14) Dong, Z. J.; Pu, Y. P.; Shi, X.; Hu, Y.; Wang, P. K.; Sun, Z. X.; Liu, X. Y. Dielectric properties of $(1\text{-}x)BaTiO_3$-$xBaFe_{12}O_{19}$ composite ceramics. *Ferroelectrics.* **2015**, *489*, 1−10.

(15) Zang, J. D.; Li, M.; Sinclair, D. C.; Frömling, T.; Jo, W.; Rödel, J. Impedance spectroscopy of $(Bi_{1/2}Na_{1/2})TiO_3$-$BaTiO_3$ based high-temperature dielectrics. *J. Am. Ceram. Soc.* **2014**, *97*, 2825−2831.

(16) Zang, J. D.; Li, M.; Sinclair, D. C.; Jo, W.; Rödel, J. Impedance spectroscopy of $(Bi_{1/2}Na_{1/2})TiO_3$-$BaTiO_3$ ceramics modified with $(K_{0.5}Na_{0.5})NbO_3$. *J. Am. Ceram. Soc.* **2014**, *97*, 1523−1529.

(17) Israel, C.; Petrov, V. M.; Srinivasan, G.; Mathur, N. D. Magnetically tuned mechanical resonances in magnetoelectric multilayer capacitors. *Appl. Phys. Lett.* **2009**, *95*, No. 072505.

(18) Nan, C. W. Magnetoelectric effect in composites of piezoelectric and piezomagnetic phases. *Phys. Rev. B* **1994**, *50* (9), 6082−6088.

(19) Andrew, J. S.; Starr, J. D.; Budi, M. A. K. Prospects for nanostructured multiferroic composite materials. *Scripta Mater.* **2014**, *74*, 38−43.

(20) Yao, Y. P.; Hou, Y.; Dong, S. N.; Huang, X. H.; Yu, Q. X.; Li, X. G. Influence of magnetic fields on the mechanical loss of Terfenol-D/$PbZr_{0.52}Ti_{0.48}O_3$/Terfenol-D laminated composites. *J. Alloy. Compd.* **2011**, *509*, 6920−6923.

https://doi.org/10.1021/acsomega.2c05975
ACS Omega 2022, 7, 45381−45385